Supplementary Information for

Implementation of the MOSAIC Aerosol Module into the Canadian Air Quality Model GEM-MACH

Kirill Semeniuk, Ashu Dastoor and Alex Lupu

Corresponding author: Kirill Semeniuk

Kirill.Semeniuk@ec.gc.ca

This PDF file includes:

Supplementary text

Figures S1 to S13

SI References

S1. Model-Observation Correlation Analysis

Model-observation correlation plots are presented here for all four model simulations for monthly-binned daily PM2.5 sulfate, nitrate and ammonium. Observational data is from station networks referenced in the article: CSN, IMPROVE and NAPS.

Figures S1-S3 show results for the MOSAIC reference simulation. Figures S4-S6 are for the CAM reference simulation. Simulations with Emerson et al. (2020) dry deposition parameters with MOSAIC are shown in Figures S7-S9 and with CAM in Figures S10-S12.

For sulfate, the reference CAM and MOSAIC results are very similar. The largest scatter occurs winter and spring (January-April and December). There is a tendency for model sulfate to have progressively smaller values than observations as the concentration decreases towards 0.1 ug/m3. The low bias in MOSAIC compared to CAM noted in the main article is also apparent.

In the case of CAM, the nitrate deviation to excessively low values for concentrations approaching 0.1 ug/m3 is striking. It is most prominent from March to October. In the case of MOSAIC, this deviation is substantially reduced and there is much less scatter. However, MOSAIC has a high bias relative to observations during most months.

For ammonium, CAM and MOSAIC show the same trend to excessively high values as concentrations decrease to 0.1 ug/m3. At many station locations, the model concentrations remain above 0.1 ug/m3 when observed values approach 0.01 ug/m3. Both aerosol schemes show a high bias in the full concentration range for every month of the year. But MOSAIC has a reduced high bias compared to CAM.

MOSAIC with Emerson dry deposition parameters result in a decrease in the bias relative to observations for sulfate and nitrate (Figs. S1-S2 vs. Figs. S7-S8). The modest sulfate low bias is essentially removed. The much more pronounced nitrate high bias is substantially reduced. For ammonium (Fig. S3 vs. Fig. S9) there is an increase in the high bias. The change in the dry deposition parameters does not affect the low bias at small concentrations which appears as a skew towards the observation axis for sulfate and nitrate, and as a skew towards the model axis for ammonium.

The effect of the Emerson parameters on CAM sulfate, nitrate and ammonium (Figs. S4-S6 vs. Figs. S10-S12) is to marginally increase concentrations in the low end of the range and to decrease them in the high end of the range. This is most apparent in fall, winter and spring months. This indicates that low concentrations have a higher association with smaller particle sizes and vice versa.

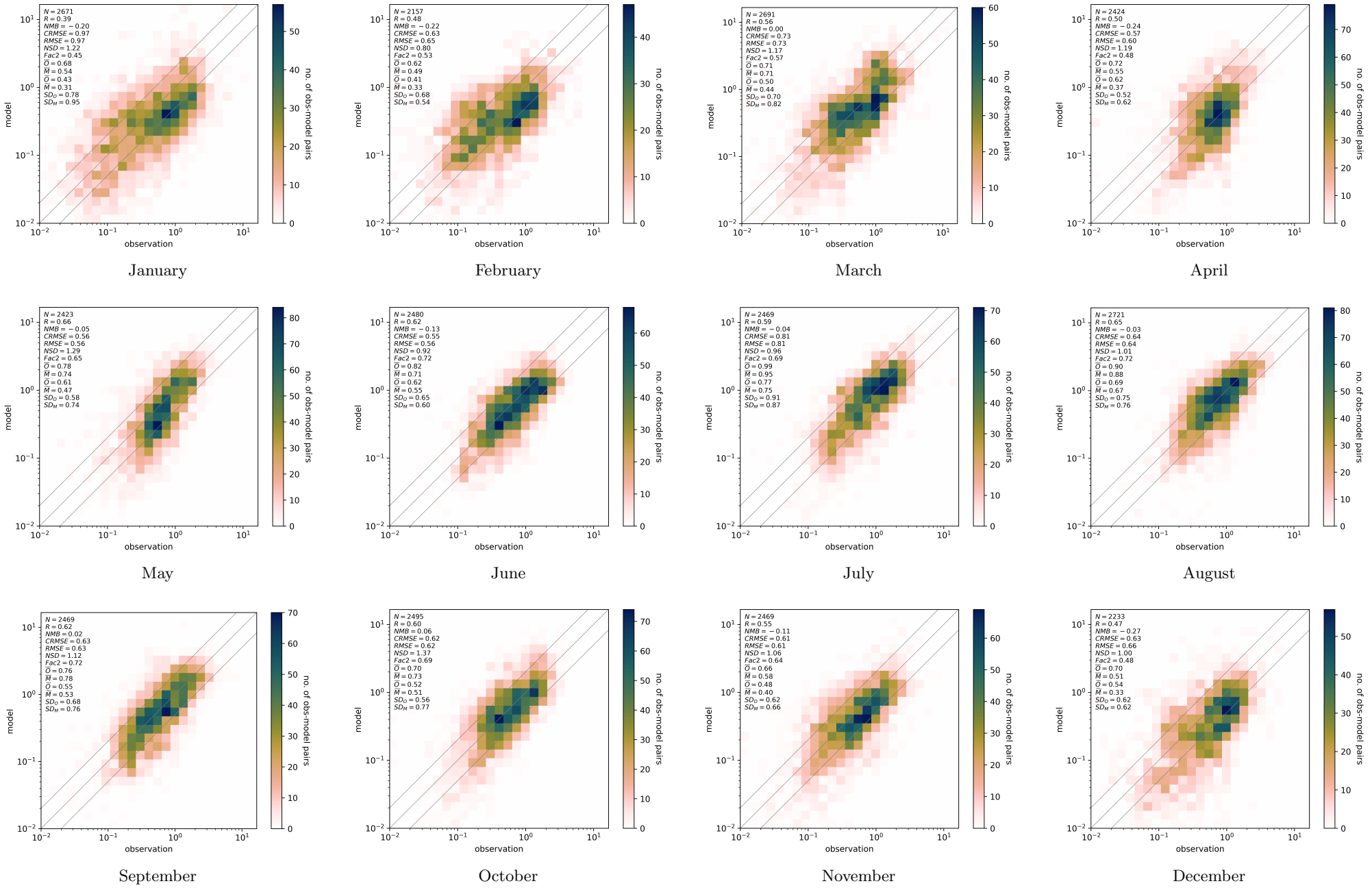

Figure S1: REF MOSAIC Daily PM2.5 SO_4 ($\mu g/m^3$) CSN + IMPROVE + NAPS

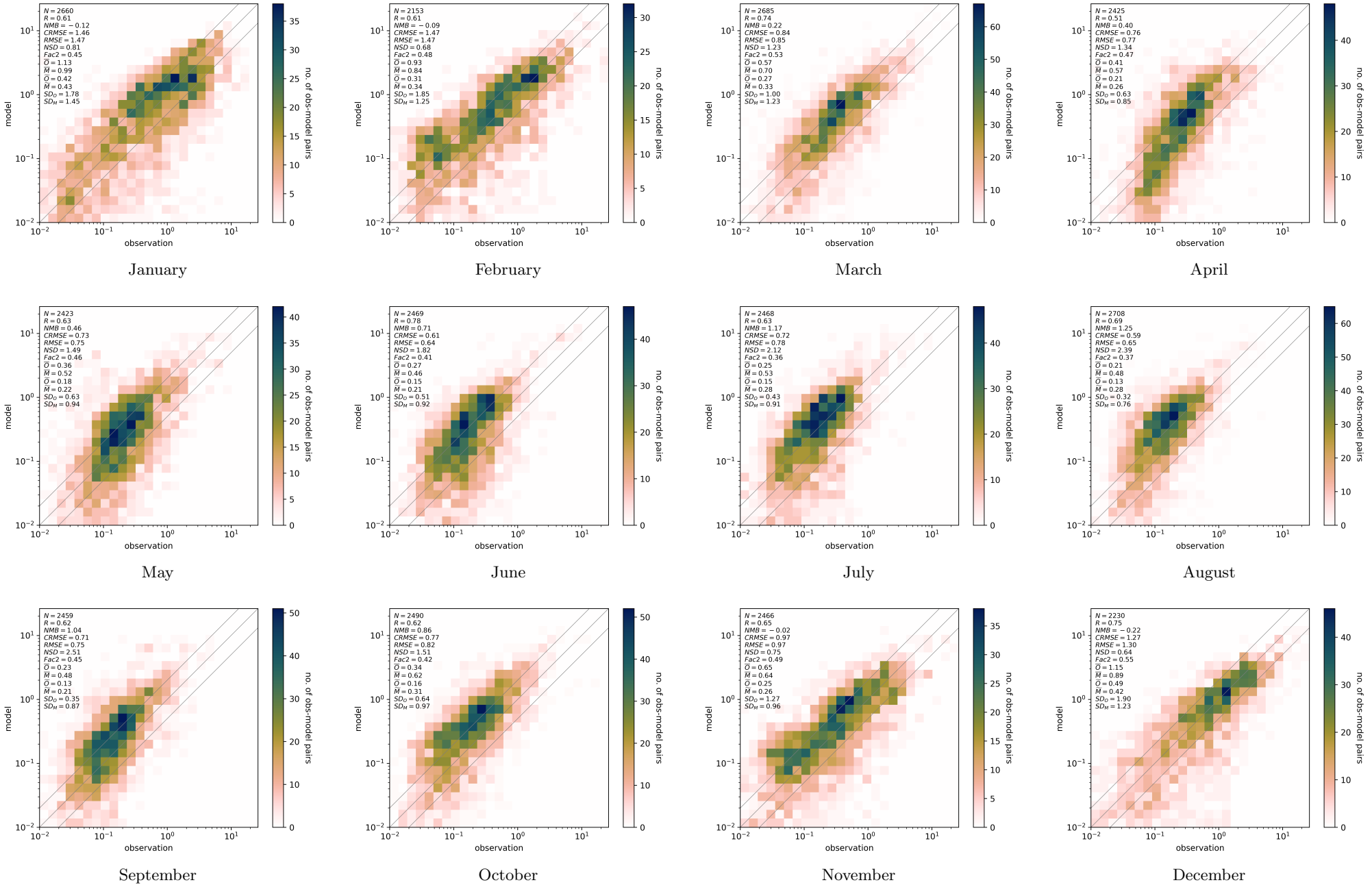

Figure S2: REF MOSAIC Daily PM2.5 NO_3 ($\mu g/m^3$) CSN + IMPROVE + NAPS

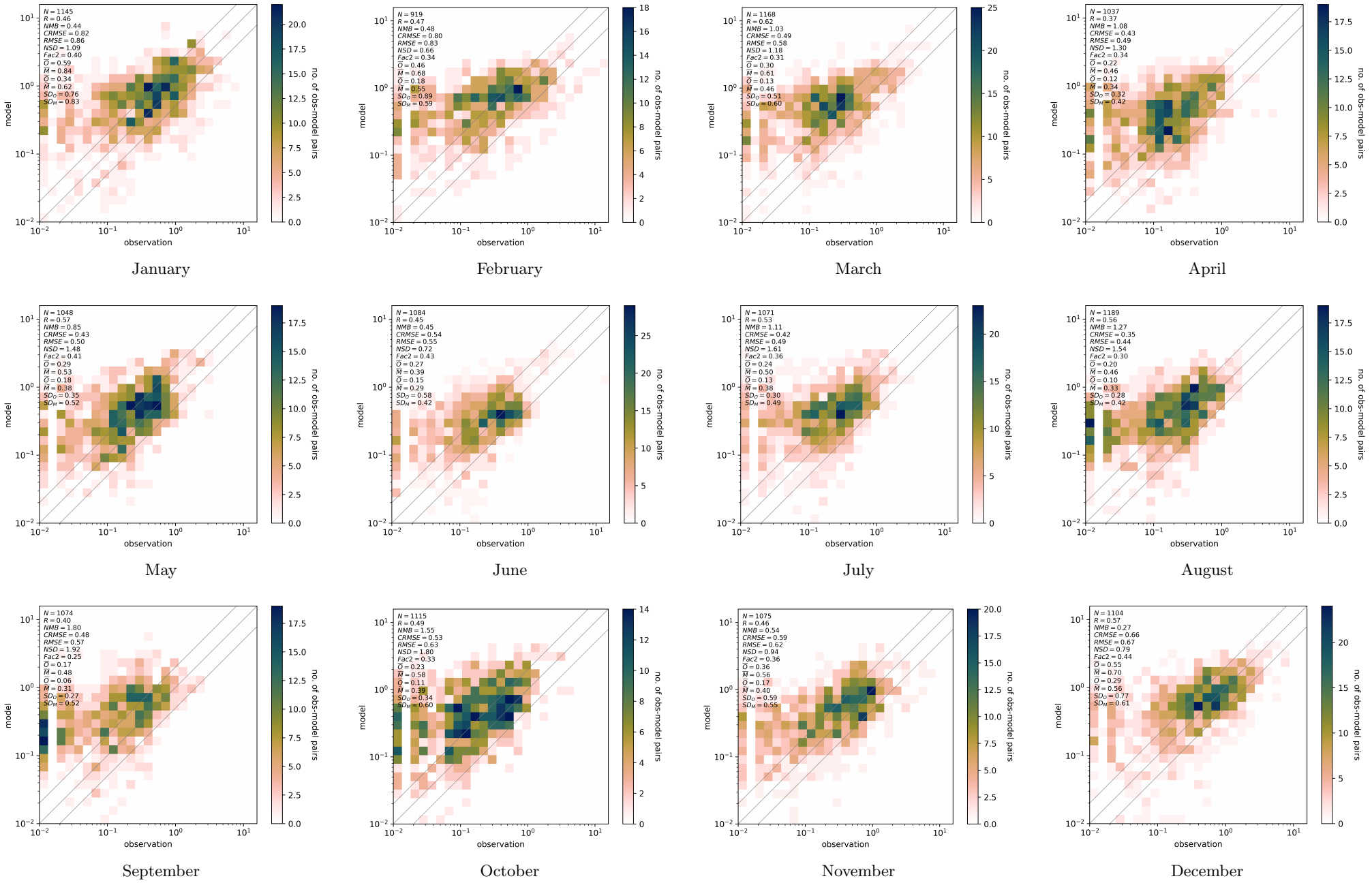

Figure S3: REF MOSAIC Daily PM2.5 NH_4 ($\mu g/m^3$) CSN + NAPS

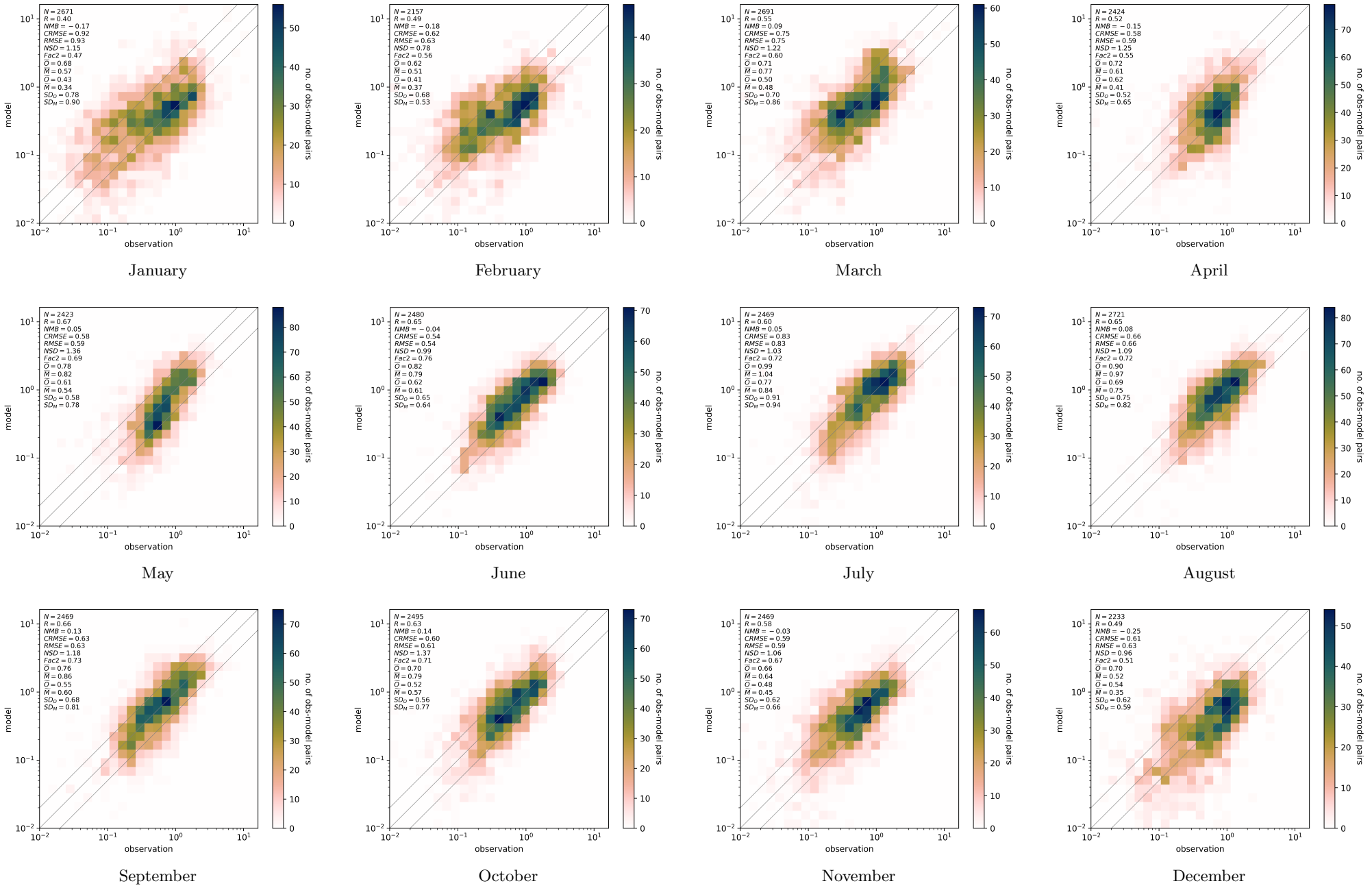

Figure S4: REF CAM Daily PM2.5 SO_4 ($\mu g/m^3$) CSN + IMPROVE + NAPS

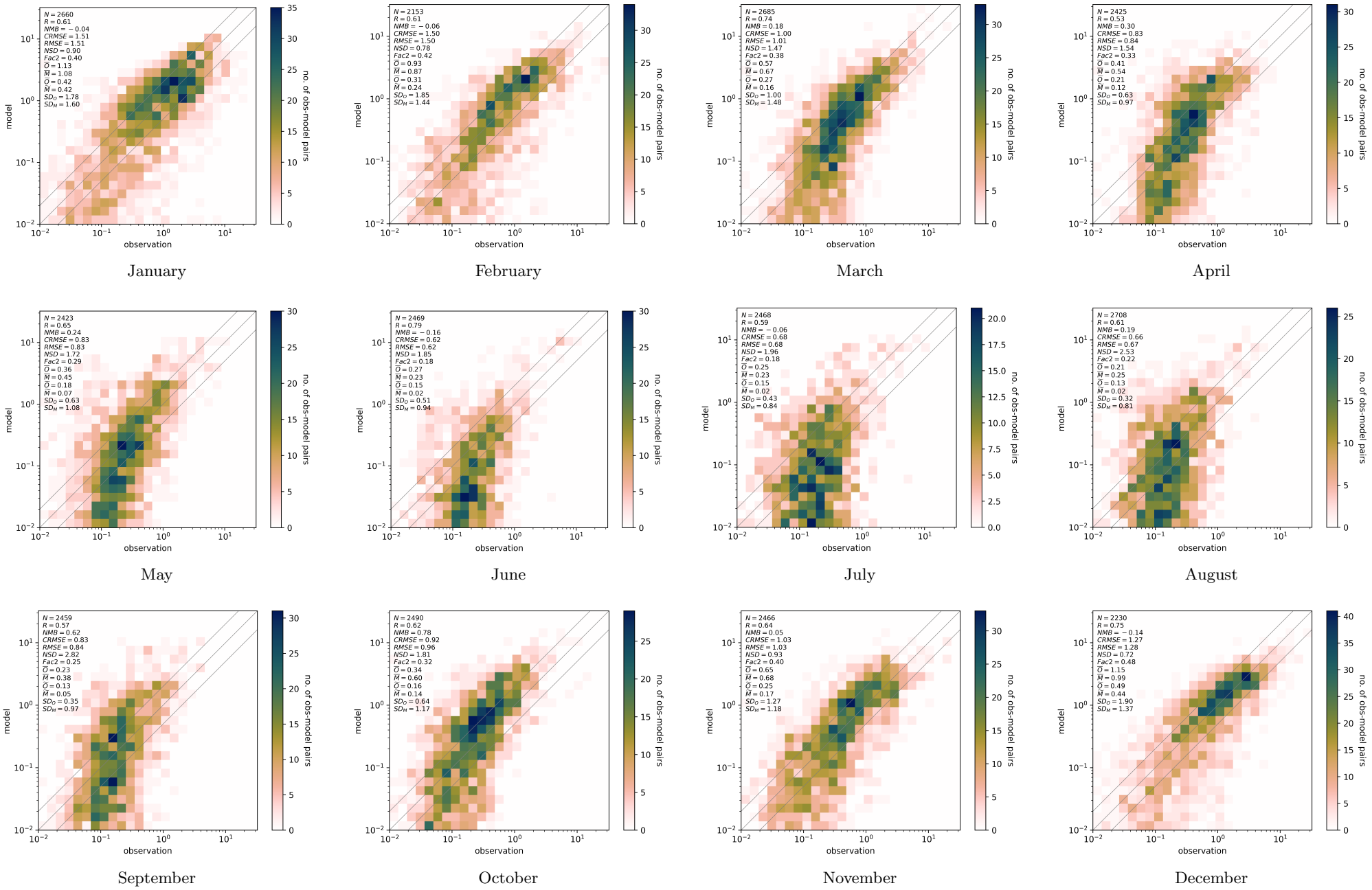

Figure S5: REF CAM Daily PM2.5 NO_3 ($\mu g/m^3$) CSN + IMPROVE + NAPS

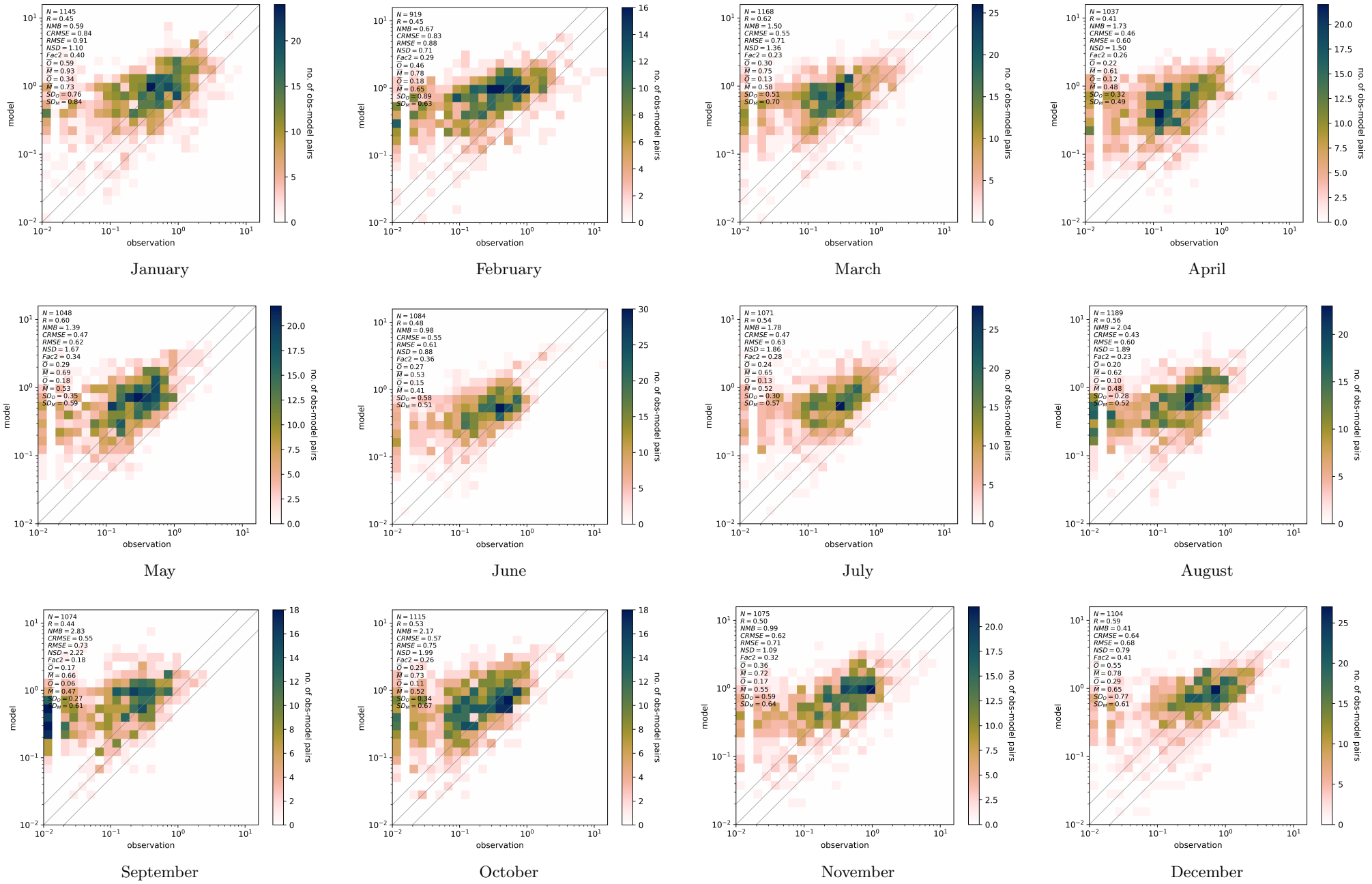

Figure S6: REF CAM Daily PM2.5 NH_4 ($\mu g/m^3$) CSN + NAPS

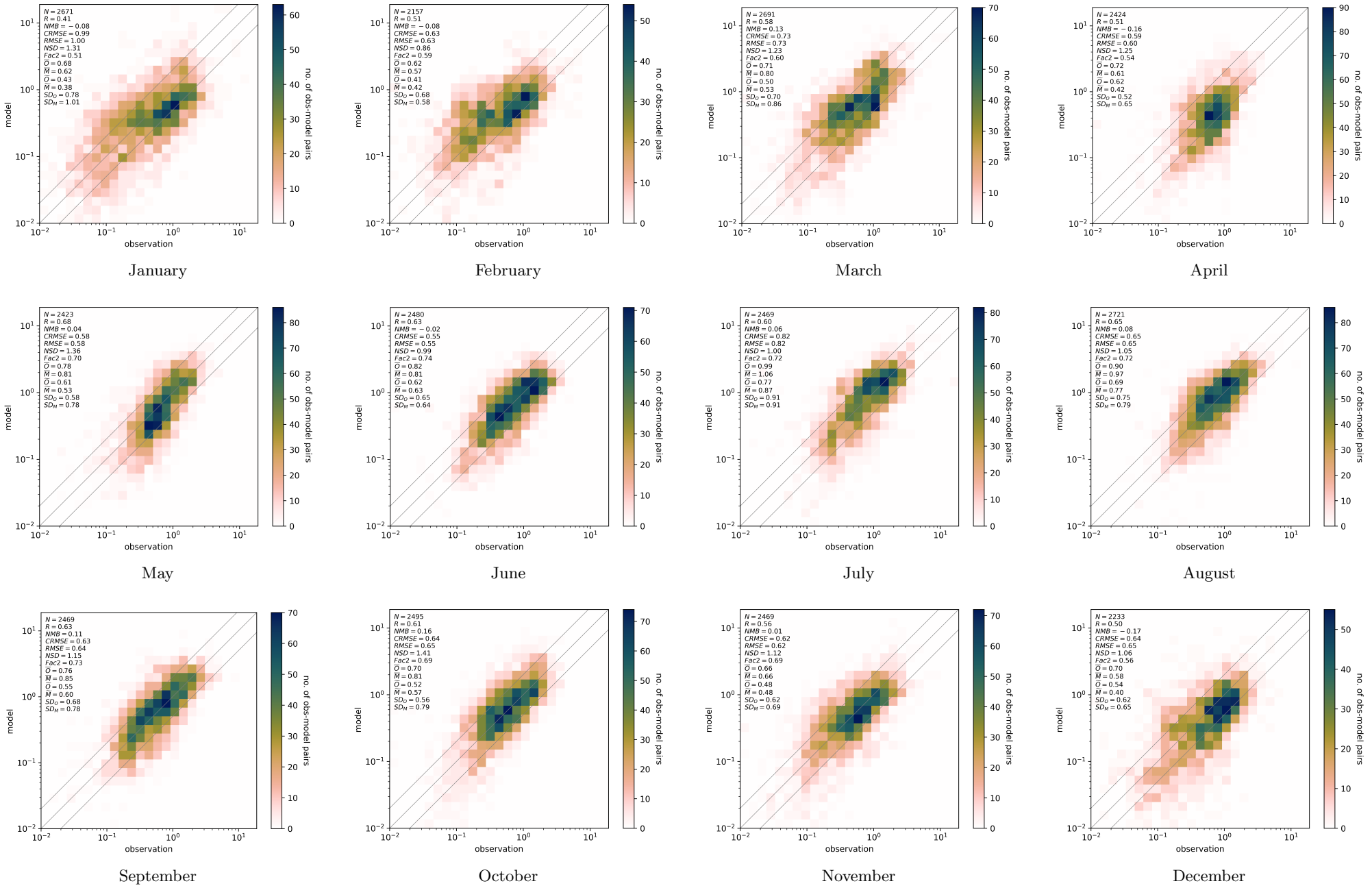

Figure S7: EMR MOSAIC Daily PM2.5 SO_4 ($\mu g/m^3$) CSN + IMPROVE + NAPS

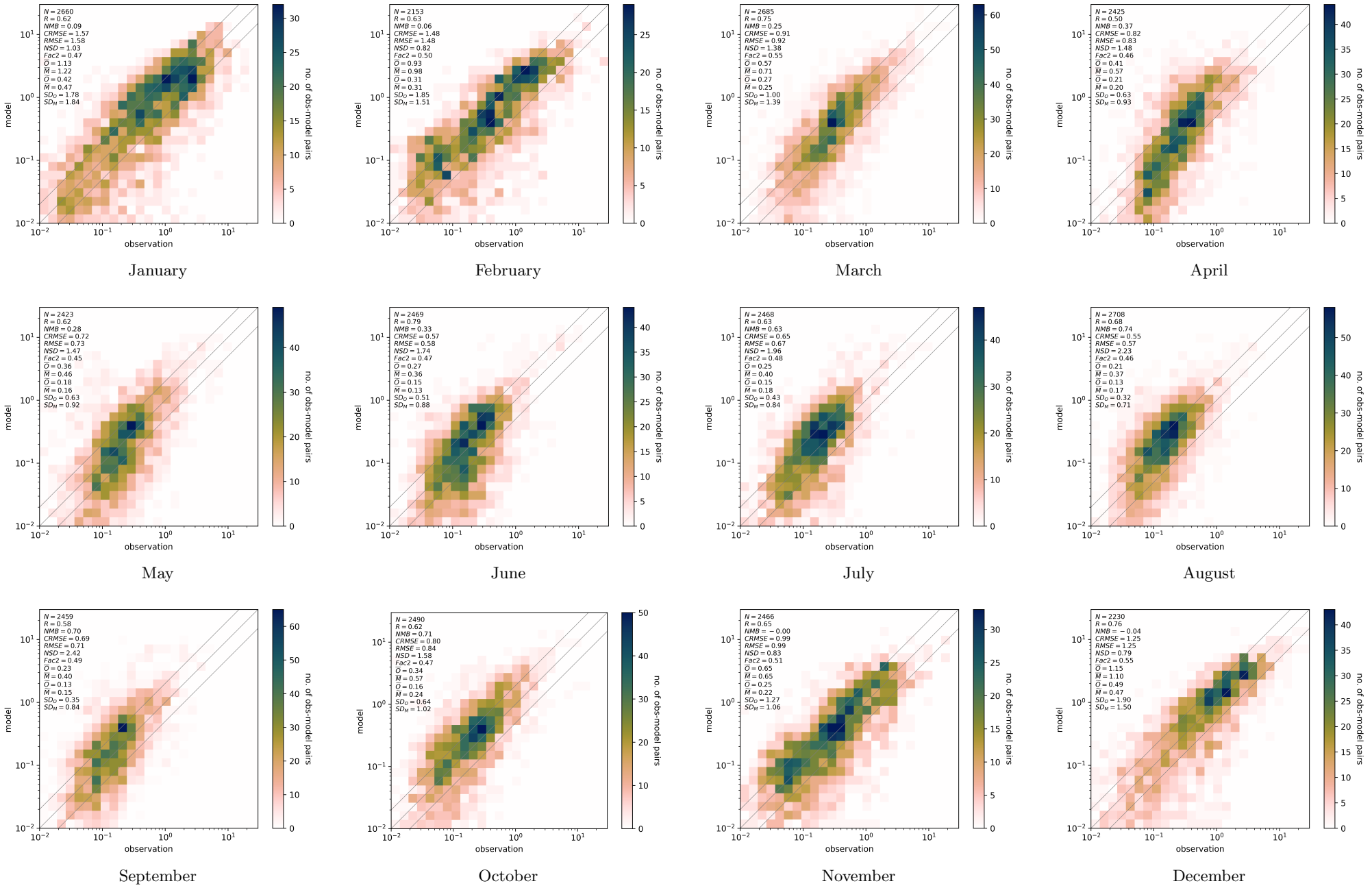

Figure S8: EMR MOSAIC Daily PM2.5 NO_3 ($\mu g/m^3$) CSN + IMPROVE + NAPS

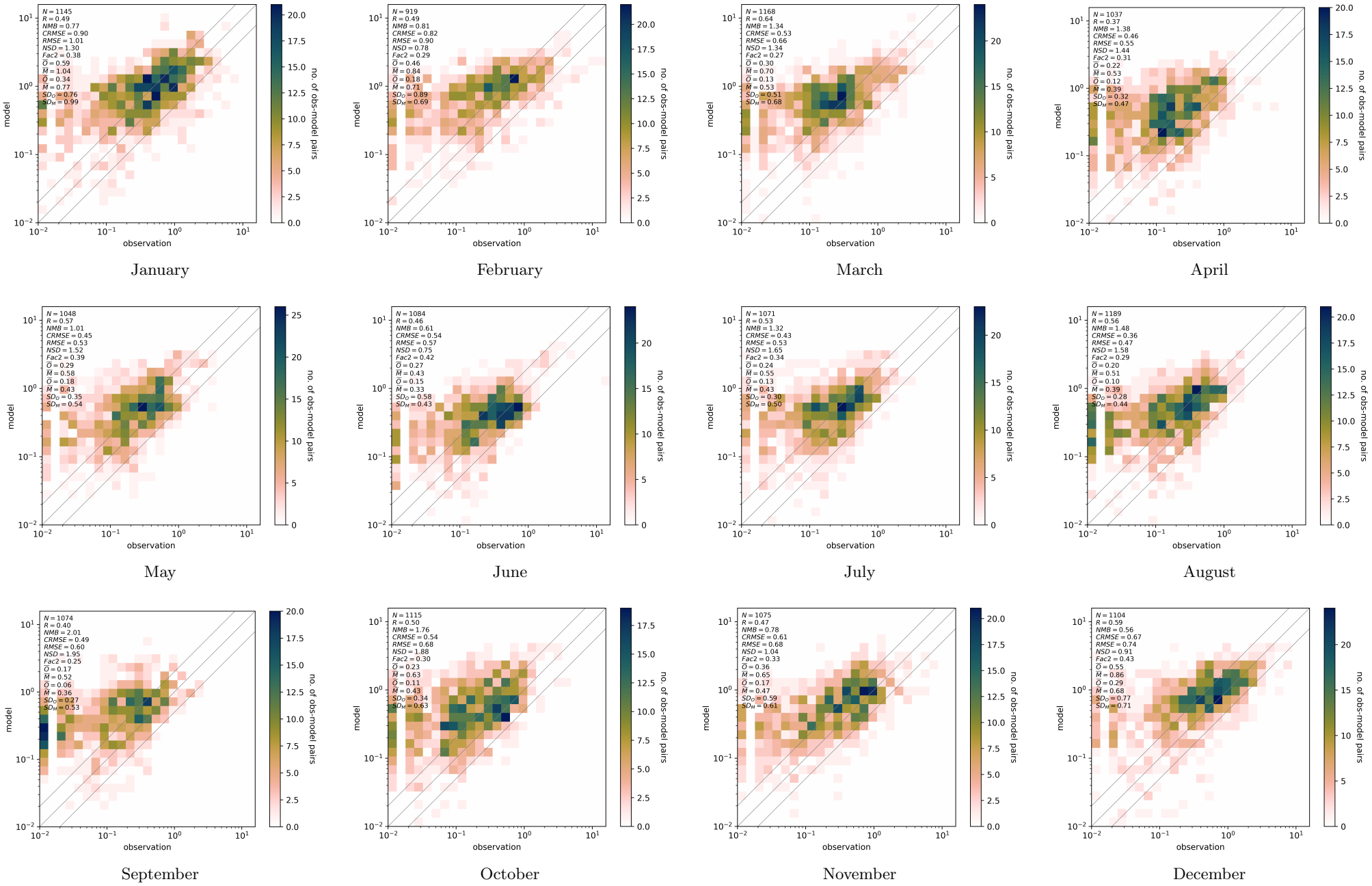

Figure S9: EMR MOSAIC Daily PM2.5 NH_4 ($\mu g/m^3$) CSN + NAPS

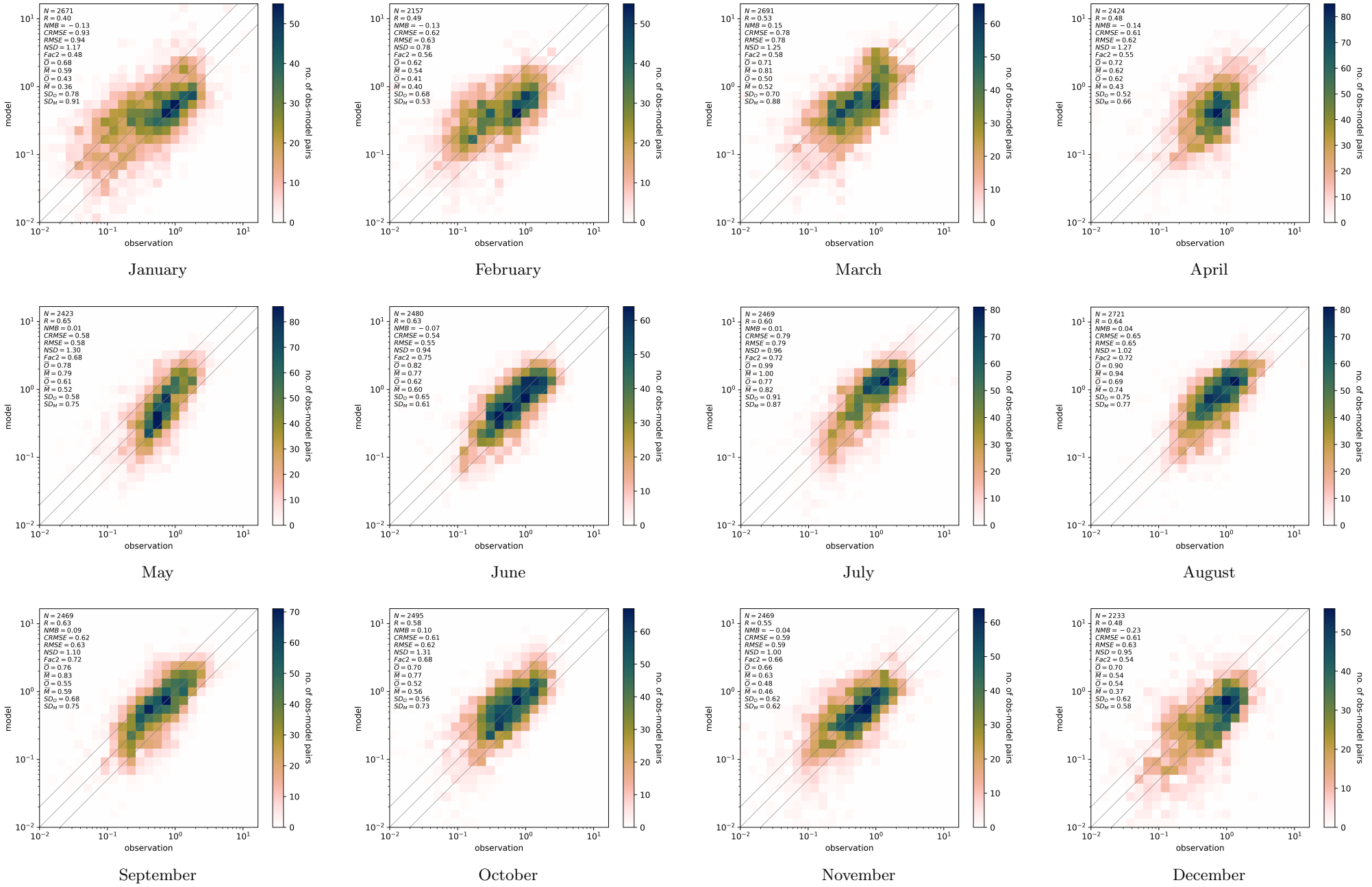

Figure S10: EMR CAM Daily PM2.5 SO_4 ($\mu g/m^3$) CSN + IMPROVE + NAPS

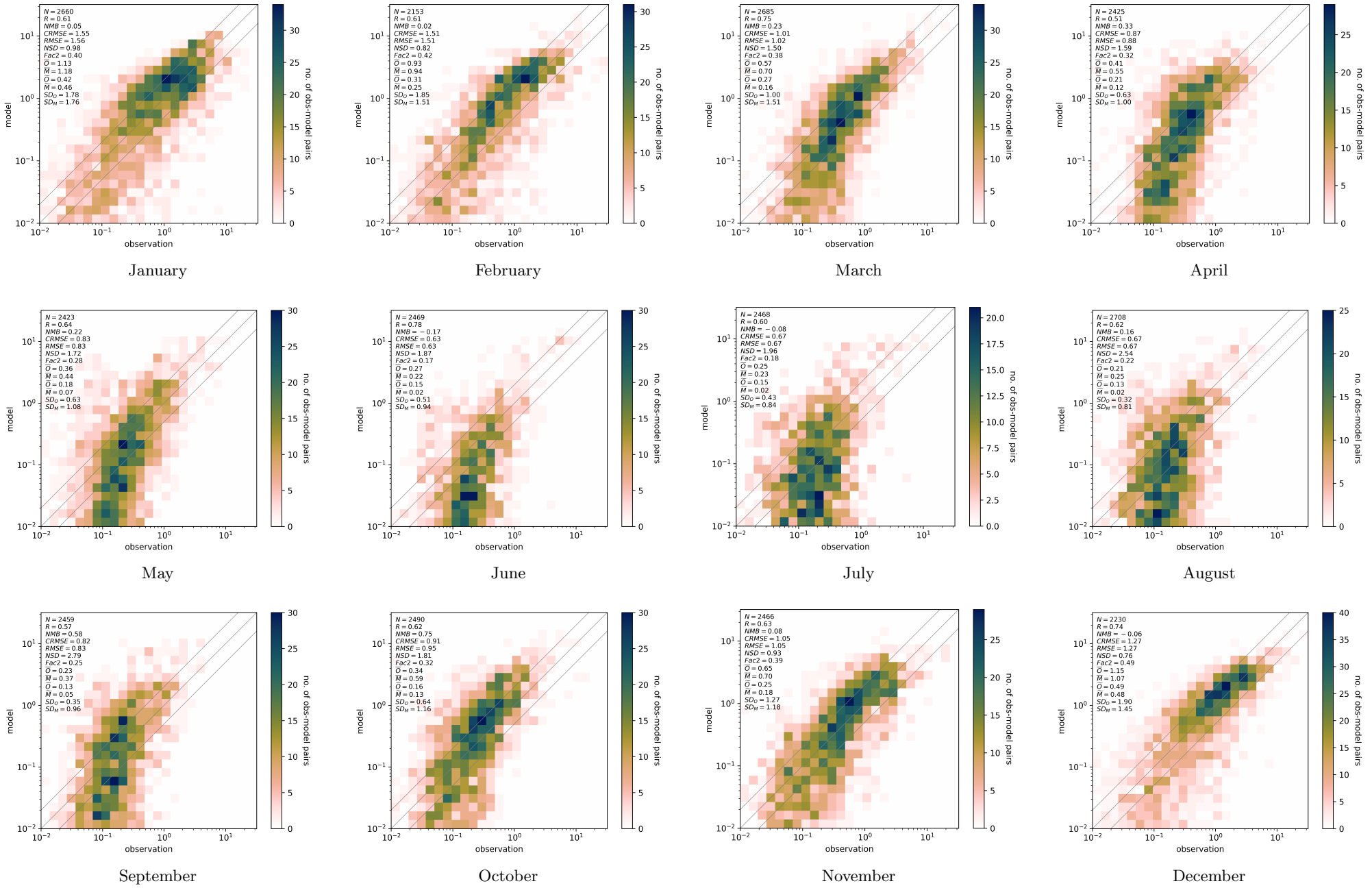

Figure S11: EMR CAM Daily PM2.5 NO_3 ($\mu g/m^3$) CSN + IMPROVE + NAPS

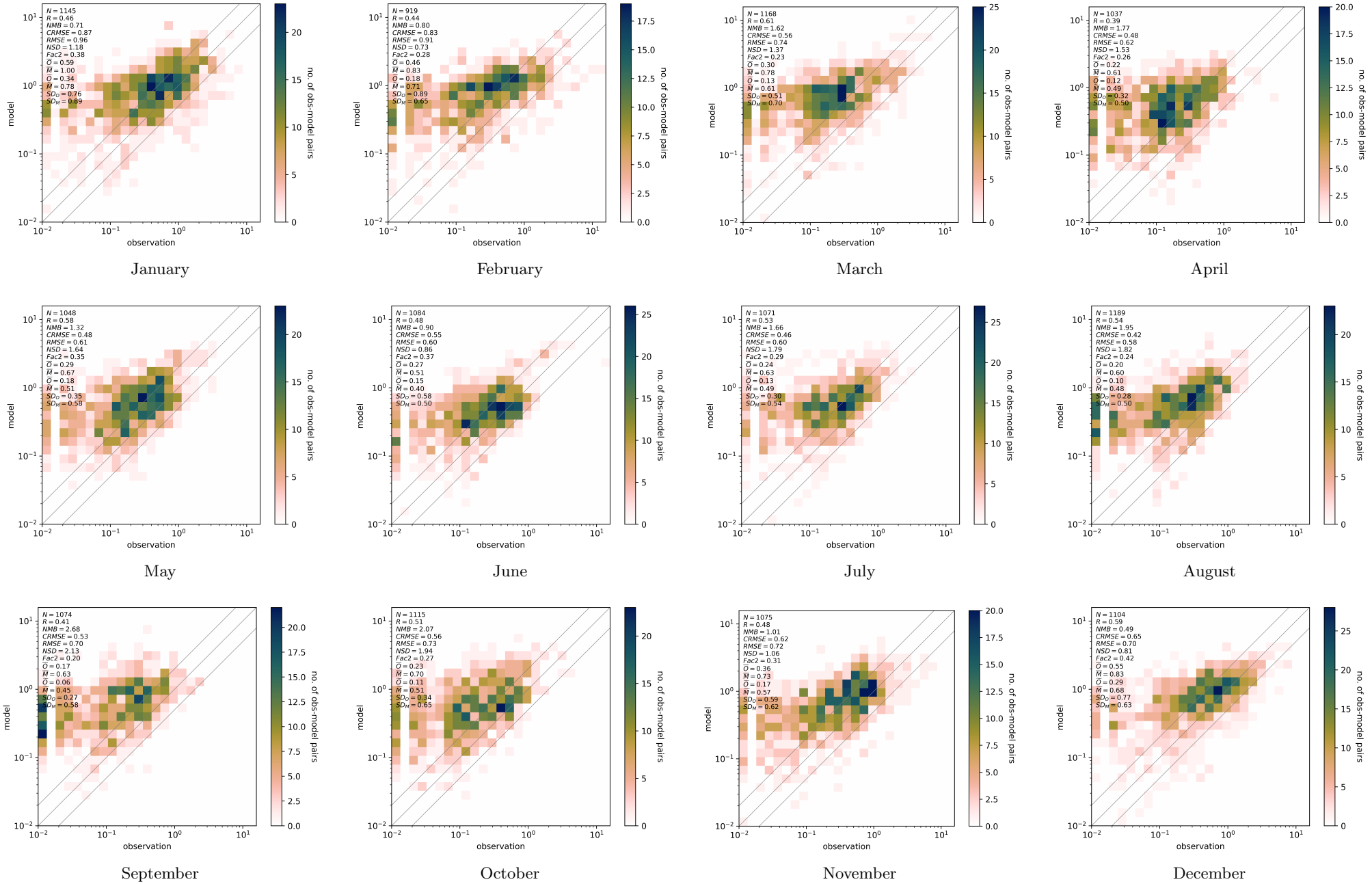

Figure S12: EMR CAM Daily PM2.5 NH_4 ($\mu g/m^3$) CSN + NAPS

S2. Gas Phase Chemical Species Comparison Between Model and Station Observations.

The reference case MOSAIC and CAM monthly and station average NH_3, HNO_3, SO_2, O_3 and NO_x for the four regions defined in the article text (Figure 4) are presented in figure S13. Nitric acid observations are combined from the Clean Air Status and Trends Network (CASTNET, https://www.epa.gov/castnet) and the Canadian Air and Precipitation Network (CAPMoN, https://www.canada.ca/en/environment-climate-change/services/air-pollution/monitoring-networks-data/canadian-air-precipitation.html). Ammonia observations are combined from the Ammonia Monitoring Network (AMON, https://nadp.slh.wisc.edu/networks/ammonia-monitoring-network) and the National Air Pollution Surveillance Program (NAPS, https://open.canada.ca/data/en/dataset/1b36a356-defd-4813-acea-47bc3abd859b). Sulfur dioxide, ozone and NO_x observations are from combined Air Quality System (AQS, https://www.epa.gov/aqs) and NAPS data.

In the case of ammonia, MOSAIC runs show slightly higher values throughout the year and in all regions with no visible variation in the difference between regions. This is consistent with the lower ammonium levels compared to CAM (Figure 6). Nitric acid shows the most pronounced difference with MOSAIC runs having lower values than CAM runs especially in regions NA1 and NA2. These regions are affected by air mass processed over oceans. The mid-continental region NA4, which has less anthropogenic pollution, has the smallest difference between the two aerosol models. The relatively polluted region NA3 shows an intermediate difference. For either aerosol option the model overestimates HNO_3 for most of the year in regions NA2-4 with late summer and early fall having the largest excess. Region NA1 stands out as having underestimation in summer but an overall better fit to observations over the year compared to the other regions for CAM. The MOSAIC option is biased low compared to CAM and observations in this region.

The additional cation constituents in MOSAIC compared to CAM result in increased uptake of HNO_3 by particulate and subsequent removal by dry and wet deposition. This is especially apparent over the oceans where sea salt sodium forms $NaNO_3$ and HCl is degassed. This leads to lower nitric acid concentrations at the surface over the oceans and regions NA1 and NA2 which experience inland air mass transport. In region NA1 there is predominant transport from the Pacific Ocean due to the prevailing westerlies. Region NA2 is also characterized by substantial transport in spring and summer from the Gulf of Mexico (e.g., Wang et al., 1998). By contrast, region NA3 is in the continental outflow zone over the Atlantic Ocean and experiences sporadic inland transport during coastal storm events. The MOSAIC low bias in HNO_3 and high bias in nitrate (Figure 6) in regions NA1 and NA2 is at least partly linked to the Gong-Monahan sea salt emission scheme which produces excessive sea salt emissions compared to other models and to observations (Spada et al., 2013). However, organics are likely to play a part as well in limiting partitioning of nitric acid into sea salt particulate. Sea salt particles have been observed with substantial organic coatings (e.g., Wang et al., 2017). Such organic aerosol processes are not represented in GEM-MACH.

For either aerosol scheme, the model has substantially less ammonia than observations in all four regions. This can be partially explained by excessive partitioning of NH_3 into the particle phase due to lack of any representation of interference from organic constituents in the aerosol sub-models. But it is likely that agricultural and ocean biogenic emissions of NH_3 are underestimated. The latter is certain since the model has no ammonia emissions over the ocean outside of the

Mississippi delta. However, ocean emissions of ammonia are not insignificant (e.g., Paulot et al., 2015; 2020). This will affect region NA1 in particular. Region NA2 is close to the boundary of the model domain which will result in the chemical boundary condition exerting a more pronounced influence than in the case of region NA1.

For SO_2, O_3 and NO_x the difference between MOSAIC and CAM in the REF simulations is too small to see in the figure. This is due to the lack in the model of feedback of aerosols on NO_x concentrations. The model SO_2 is excessive in all regions and for most of the year. Region NA1 shows the largest wintertime bias. This region also differs from the others in having a high bias in wintertime sulfate compared to observations (Fig. 6 in the main article). In regions NA2-4 the wintertime sulfur dioxide bias is smaller than in NA1 and this corresponds to a low bias in sulfate. It appears that there is insufficient conversion of SO2 into sulfate during winter in the model. This putative conversion deficit is reduced in the rest of the year and contributes to the high bias in sulfate seen in summer and fall in regions NA2-4. However, the variation in sulfate from month to month is not simply correlated with SO_2 concentrations and other processes are involved.

The difference between the EMR and REF runs for these gases for both MOSAIC and CAM show essentially no difference and are not shown.

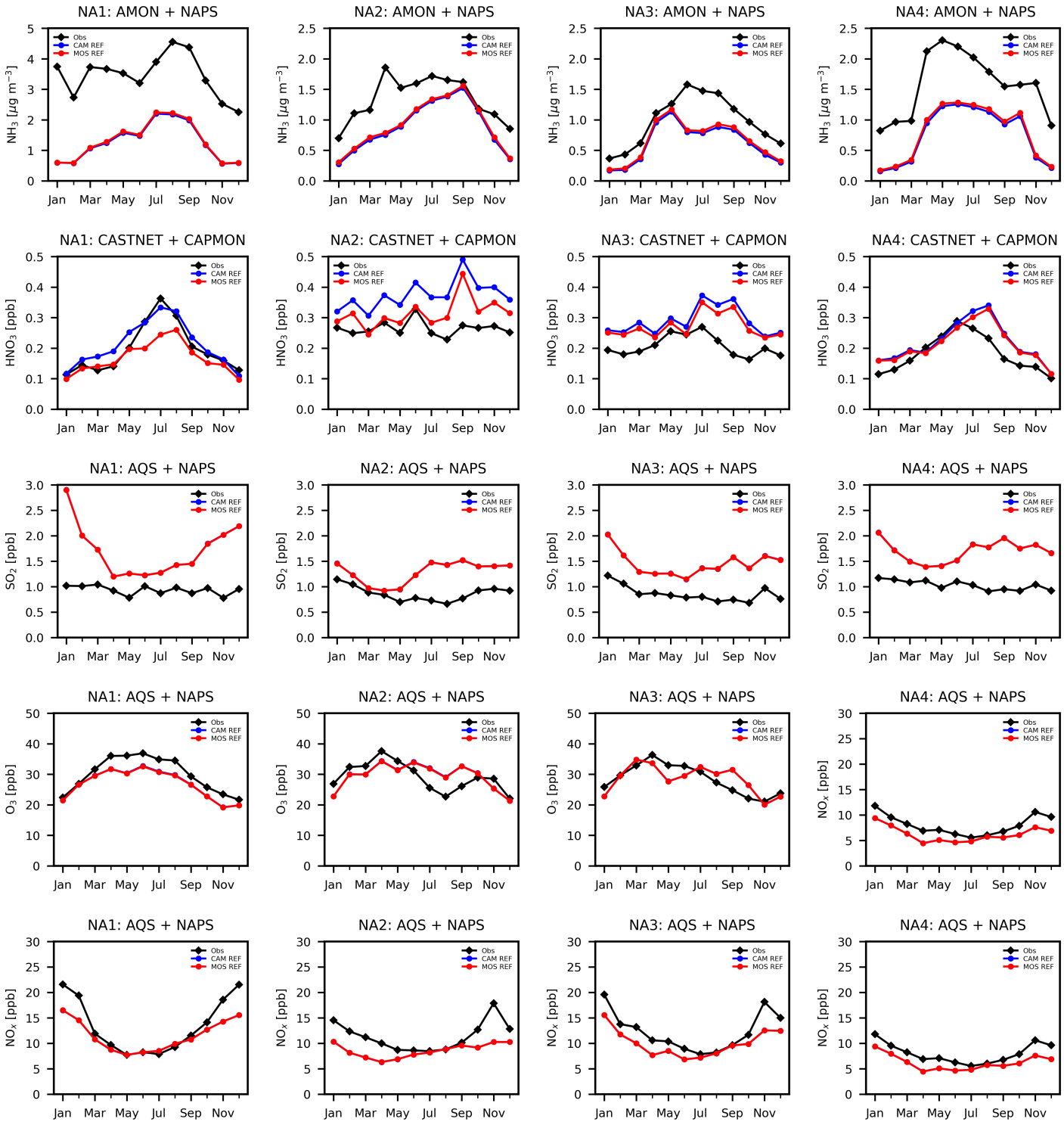

Figure S13: Regional reference run month and station mean time series of NH_3 (1^{st} row), HNO_3 (2^{nd} row), SO_2 (3^{rd} row), O_3 (4^{th} row) and NO_x (5^{th} row). MOSAIC (red), CAM (blue) and observations (black) are shown. Units for NH_3 are $\mu g/m^3$ and for the rest are ppb as dictated by station data.

SI References

1. Emerson, E. W., Hodshire, A. L., DeBolt, H. M., Bilsback, K. R., Pierce, J. R., McMeeking, G. R., and Farmer, D. K. (2020), Revisiting particle dry deposition and its role in radiative effect estimates, PNAS, 117(42), 26076–26082, doi:10.1073/pnas.2014761117.
2. Wang, W., Nowlin Jr., W. D., and Reid, R. O. (1998), Analyzed surface meteorological fields over the Northwestern Gulf of Mexico for 1992-1994: mean, seasonal, and monthly patterns, Mon. Wea. Rev., 126(11), 2864-2883, doi:10.1175/1520-0493(1998)126<2864:ASMFOT>2.0.CO;2.
3. Spada, M., Jorba, O., Perez Garcia-Pando, C., Janjic, Z., and Baldasano, J. M. (2013), Modeling and evaluation of the global sea-salt aerosol distribution: sensitivity to emission schemes and resolution effects at coastal/orographic sites, Atmos. Chem. Phys., 13, 11735-11755, doi:10.5194/acp-13-11735-2013.
4. Wang, H., Wang, X., Yang, X., Li, W., Xue, L., Wang, T., Chen, J. and Wang W. (2017), Mixed chloride aerosols and their atmospheric implications: a review, Aer. Air Qual. Res., 17, 878-887, doi:10.4209/aaqr.2016.09.0383.
5. Paulot, F., Jacob, D. J., Johnson, M. T., Bell, T. G., Baker, A. R., Keene, W. C., Lima, I. D., Doney, S. C., and Stock, C. A. (2015), Global oceanic emission of ammonia: Constraints from seawater and atmospheric observations, Global Biogeochem. Cycles, 29, 1165–1178, doi:10.1002/2015GB005106.
6. Paulot, F., Stock, C., John, J. G., Zadeh, N., and Horowitz, L. W. (2020), Ocean ammonia outgassing: Modulation by CO2 and anthropogenic nitrogen deposition. Journal of Advances in Modeling Earth Systems, 12, e2019MS002026. doi:10.1029/2019MS002026.